Wave Phase based Conditional Sampling of Reynolds Stresses in the Coastal Ocean Bottom Boundary Layer

Luksa Luznik
Dept. of Mechanical Engineering
The Johns Hopkins University
Baltimore, MD, 21218, USA
lluznik@poseidon.me.jhu.edu

Roi Gurka
Department of Mechanical Engineering
The Johns Hopkins University
Baltimore, MD, 21218, USA

W.A.M. Nimmo Smith
School of Earth, Ocean and Environmental Sciences
University of Plymouth
Plymouth, Devon, PL4 8AA, UK

Weihong Zhu
Department of Mechanical Engineering
The Johns Hopkins University
Baltimore, MD, 21218,USA

Joseph Katz
Department of Mechanical Engineering
The Johns Hopkins University
Baltimore, MD, 21218, USA

Thomas R. Osborn
Department of Earth and Planetary Science
The Johns Hopkins University
Baltimore, MD, 21218, USA

ABSTRACT

The paper discussed methods for conditionally sample Reynolds stresses measured in the bottom boundary layer of the coastal ocean based on the wave phase. Since wave contamination prevents direct calculation of stresses, PIV data is used for estimating the stresses from the second order structure functions of the spatial velocity distributions. Hilbert transforms of pressure signal and spatially averaged velocity are used for determining the wave phase. For most cases, a phase mismatch occurs when the wave amplitude is small or when the turbulence is high. The data are then sub-sampled, keeping only points for which the phase difference is less than 35^0. Such sub-sampling has little impact on the Reynolds stresses. Conditional sampling shows that all the Reynolds stresses vary with wave phase, but the variations of the shear stress are particularly high. Except for a consistent minimum in <u'u'> at the phase of maximum wave induced velocity, there are significant differences between trends of data recorded at different elevations and/or times.

INTRODUCTION

Proper modeling of circulation, sediment transport, pollutant dispersal and biological processes in the coastal ocean require knowledge on the characteristics of turbulence in the bottom boundary layer. Point measurement techniques that have already been used extensively for measuring the turbulence in the coastal ocean are adversely affected by contamination from surface waves. Although the waves typically have much larger spatial scales than the turbulence, the frequency of the orbital wave motion falls within the turbulence spectrum, since the wave speed is much higher than the typical flow. Thus, separating the wave-induced motion from turbulence in the signal of a point sensor is virtually impossible, and a major challenge even in laboratory conditions (Thais and Magnaudet, 1996). Furthermore, since the Reynolds shear stress is a correlation between streamwise and vertical velocity components, the alignment of the instrument relative to the mean flow in an environment with waves is critical. When the instrument is misaligned, both its vertical and horizontal components are "contaminated" by the projection of the wave-induced horizontal velocity component. This wave effect dominates the velocity correlations, making the direct stress measurements impossible. Consequently, Trowbridge (1998) introduces a technique based on simultaneous measurements using two spatially separated sensors, and estimating the stresses from the covariance (2^{nd} order structure function) of the corresponding velocity components. His approach clearly illustrates the advantage in performing simultaneous velocity measurements at multiple points, which makes Particle Image Velocimetry (PIV) a particularly attractive option for characterizing the flow and turbulence in the coastal ocean.

Over the last several years we have been implementing the Trowbridge method to calculate the Reynolds stresses using PIV data (Nimmo Smith et al., 2002, 2005, Osborn et al., 2005). To examine the effect of waves on the turbulence, Osborn et al. (2005) uses the Hilbert transform to determine the instantaneous phase of the wave, and then conditionally samples the Reynolds stresses based on this phase. The data used in this analysis were obtained under conditions of weak mean flow, and wave induced velocity amplitude that is comparable or higher than the mean velocity. The analysis shows significant variations in Reynolds stresses and mean current with phase. These trends cast some doubts upon the assumption under which the second order structure function approach is formulated, namely that there is no correlation between the wave orbital motion and turbulence. In the present paper we attempt to use the same method to examine a data set with higher mean flow and turbulence levels. As the results show, determining the wave phase becomes a challenge. We use and compare several approaches and data sources, including velocity and pressure time series for calculating the wave phase. The comparisons indicate that in some cases one can obtain reliable estimates of phase and conditionally sampled Reynolds stresses, while in others, especially when the turbulence levels are high, there is a room for improvement.

MEASUREMENTS

Instrumentation

The submersible PIV system, illustrated in figure 1, consists of two principal components, one located on the ship, and the other submerged. The shipboard component consists of a laser, associated optics, acquisition and control computers, and high-speed disk arrays for data storage. The light source is a dual head, dye laser with pulse duration of 2 μs and maximum output of 350 mJ/pulse at wavelength of 594 nm. The laser beam is split and transmitted through two 60 m long optical fibers to the submerged system, which contains two independent probes with laser sheet forming optics. The images are recorded using two CCD cameras each with 2048x2048 pixels resolution, operating at 3 Hz. The cameras are equipped with electronic image shifters that resolve the directional ambiguity problem while recording two-exposure images. The system configured for the deployments discussed in this paper has cameras located 120 cm from the light sheet, each with a sample areas of 35x35 cm^2, and are separated horizontally by 31 cm. The time delay between the exposures is adjusted according to the mean streamwise velocity, and in most cases is 8 ms. The cameras, light sheet probes and a suite of supporting environmental sensors are rigidly mounted on turntable located on the top of a profiling platform that has an extension capability of 10 meters. Prior to each series of measurements, the plane of the laser sheet is aligned with the mean flow. Further details on the PIV system and auxiliary instruments can be found in Nimmo Smith et al. (2002). We only mention the ParoScientific Digiquartz, Model 6100A, precision pressure transducer, which is operating at 6.7 Hz, whose records are used in the analysis that follows.

The acquired images are analyzed using an in-house developed correlation analysis code (Roth et al., 2001, Nimmo Smith et al., 2005). The interrogation windows size is 64x64 pixels, which with 50% overlap between windows yields 63x63, 2D instantaneous velocity vectors. The typical uncertainty in instantaneous velocity is about 2%. Since we rely on natural seeding, in some cases part of the sample area does not have enough particles for calculating the velocity. Instantaneous vector maps that contain less than 70% of the total number of vectors are not used in subsequent analysis. Due to the large field of view, the PIV data is calibrated to compensate for the variations in magnification across the sample area, and for effects of out of plane motion, as discussed in Nimmo Smith et al. (2002).

Flow Conditions

The measurements described here were performed from 6-20 June 2003, during the cruise aboard R/V Cape Hatteras, to the vicinity of the South Atlantic Bight Synoptic Offshore Observational Network (SABSOON). The test site was located on the continental shelf, along the Georgia coast. The mean water depth was 23 m, with bottom slope of 3/700 m, and the seabed consisted of sand and broken shells. The mean depth-averaged velocity, as measured by an onboard Acoustic Doppler Current Profiler (ADCP), indicated strong semidiurnal tidal currents with magnitude ranging from 10 to 45 cm/s.

The PIV measurements concentrated on the bottom boundary layer, starting from 0.45 m up to 2.5 m above the bottom. Each run lasted for 20 minutes, providing 3600 PIV realizations per run. Figure 2 shows the vertical distribution of the mean streamwise velocity, $U(z)$, obtained during one night of continuous deployment for 6 hours. The data are normalized with the depth-averaged speed of the ship ADCP (the actual values are provided in the inset). At each elevation we show two profiles obtained at different phases of the tidal cycle. Runs 101 to 104 were obtained during the accelerating phase, while runs 105 to 107 during decelerating phase. Details on turbulent statistics and spectra of this data are described in Luznik et al., (2005). The pressure transducer spectra (not shown here) have a peak at 0.13 Hz i.e. the wave period is about 8 seconds. This result agrees with the data obtained from wave buoy (# 41008), located about 5 nautical miles NW of the measurement site.

DATA ANALYSIS

In the analysis that follows, the x and z coordinates, with the corresponding u and w instantaneous velocity components, denote the streamwise and wall-normal directions in the frame of reference of the PIV system. U and W denote ensemble average components, and $\langle\rangle$ represents ensemble averaging. The camera (sample area) located upstream is referred to as camera A, and the downstream camera is denoted camera B.

Reynolds Stress Estimates

The in-plane stress components $\langle u'u'\rangle$, $\langle w'w'\rangle$ and $\langle u'w'\rangle$ are estimated using the second order structure function $D_{ij}(x,r,t)$, defined as:

$$D_{ij}(x,r,t) = \left\langle [u_i(x,t) - u_i(x+r,t)][u_j(x,t) - u_j(x+r,t)] \right\rangle \quad (1)$$

where i and j identify velocity components, and r is the separation distance between two points. It can be shown (Trowbridge 1998, Osborn et al., 2005) that if r is larger than the integral scale of the turbulence, and much smaller than the wavelength of surface waves $D_{ij} \approx 2\langle u'_i u'_j \rangle$. The PIV data enables calculation of the distribution of D_{ij} as a function of the separation distance. Thus, provided that the sample areas are large enough, we can determine the values of r for which D_{ij} reaches an asymptotic value without prior knowledge of the integral scale of turbulence. Using two cameras with sample area of 35x35 cm, separated by 31 cm enables us to calculate $D_{ij}(r,t)$ for $0\ cm<r<100\ cm$. As an example, Figure 3 shows distributions of $0.5D_{ij}(r)$ for the data set recorded at the mean elevation of 0.45 m (run 101) above bottom. Three different distributions are presented for each stress component, two for r spanning over individual sample areas, and one covering separation distances across both samples. The distributions of $-0.5D_{13}$ and $0.5D_{33}$ calculated over both sample areas display asymptotic behavior with convergence starting at about r=80 cm, while $0.5D_{11}$ is not fully converged even as $r \rightarrow 1$m.

In this paper, we calculate the time series of the $D_{ij}(r,t)$ in order to study variations of Reynolds stresses with wave phase. To this end, we use the central 9x9 velocity vectors of each pair of realizations to calculate 81 values of the of the instantaneous structure function at a fixed separation distance of 0.66 m. These values are then averaged together to yield a single estimate of the structure function at each

time instant. Two points need to be kept in mind before proceeding: First, as Figure 3 shows, at this elevation and separation distance, the structure functions do not reach asymptotic values, i.e. they underestimate the corresponding Reynolds stresses. Second, as reported by Luznik et al., (2005), for the SABSOON data sets and for elevations greater than 1.5 m, all the structure functions do not converge to asymptotic values, even at the present maximum separation distance. Thus, larger separations are needed for estimating the Reynolds stresses accurately. Nevertheless, the time series of structure function can still be used for conditional sampling based on the phase of wave-induced motion.

Basis for Conditional Sampling

In an attempt to determine the wave phase, we use the Hilbert transform to convert a time series of pressure and velocity components into a complex time series of phase and amplitude. In-depth descriptions of this transform and its application in conditional sampling of unsteady phenomena are provided in Huang et al., (1998) and Hristov (1998). The Hilbert transform is applied on the time series after subtracting a 15 s running average calculated in both directions in order to produce no phase shift. The phase angle of the time series provides an estimate for the local instantaneous phase of the signal. Two data sets obtained at the same time are used as the basis for conditional sampling: the spatially averaged horizontal velocity component, as measured by the PIV system, and the time series of pressure, which represents the variations in free surface elevation. To minimize the effect of turbulence on the basis for calculating the wave phase, we spatially average the central 59x59 vectors of the instantaneous horizontal velocity over individual vector maps, and denote them as $\tilde{u}_A$ or $\tilde{u}_B$. The resulting sets of 20 minutes (3600 points) time series contain the wave signature, along with the effects of large-scale turbulence. To further reduce the turbulence effect, we also combine the data from both cameras, and denote this series as $\tilde{u}_{AB}$ ($= \tilde{u}_A + \tilde{u}_B$). The pressure signal, which is recorded at 6.7 Hz, is re-sampled at 3 Hz in order to match it with the velocity time series.

RESULTS

Hilbert Transform

In this paper we conditionally sample the data sets of Runs 101, 103 and 105, whose elevations and mean currents are presented in Figure 2. Figure 4 shows sample scatter plots of spatially averaged velocity components as a function of the instantaneous phase, as calculated from the Hilbert transform, for run 103. Figure 4a shows $\tilde{u}_A$, the spatially averaged horizontal velocity of camera A, conditionally sampled and plotted based on its own phase, Φ_{uA}. Figure 4b shows the same velocity component, this time conditionally sampled based on the phase of $\tilde{u}_{AB}$. Figure 4c shows the spatially averaged vertical velocity of camera B, $\tilde{w}_B$, conditionally sampled based on Φ_P, the phase calculated from pressure time history. From Figures 4a and b it is clear that when the same series is sampled based on different estimates of the instantaneous phase, the extent of scatter in the data changes. This example provides a qualitative indication how coherent the wave-induced motions are between the two sample areas. It also indicates that the instantaneous phase estimates used for conditional sampling vary slightly, depending on which time series is used for calculating the phase. We believe that the two main causes for the differences in phase between sample areas are: i. spatially varying effects of large-scale turbulence, and ii. since the wave direction may be inclined to the mean flow, and there may be even more than one wave propagating in different directions, the wave signatures in $\tilde{u}_A$ and $\tilde{u}_B$ become complex at times, making it difficult to define the phase. The main question is then: Can we use the velocity time series to obtain reliable estimates for the instantaneous phase?

The distribution of $\tilde{w}_B$ with Φ_P show substantial scatter. The same trend occurs if we use any of the horizontal velocity components for conditional sampling. The scatter appears to be similar if we sample based on Φ_{uAB}, and more severe if the phase is calculated based on Φ_{uA} or Φ_{uB}. However, the expected 90^0 phase shift between vertical and horizontal velocity components is still clearly evident. We believe that some of the scatter is caused by contamination of the inherently smaller wave-induced vertical velocity component with the horizontal velocity due to slight instrument misalignment. One can even attempt to determine and minimize the effect of misalignment by finding the angle that best brings the vertical and horizontal velocity components into quadrature.

Data Sub-Sampling Based on Matched Phases

After examining and comparing several time series to determine the phase, it has become evident that Φ_{uAB} is more coherent with Φ_P than phases determined from the velocity in one sample area. This agreement is not coincidental. By averaging the instantaneous velocity from two sample areas, we are extending the range of scales to 1 m, close to the integral scale of turbulence, as the structure functions indicate. Thus, the impact of turbulence on the velocity time series is expected to decrease. The pressure signal is dominated by wave-induced variations in surface elevation. Figure 5 compares Φ_{uAB} to Φ_P for run 103. Most of the data points lie in the vicinity of the 45 degrees line, but there is still significant scatter. Two symmetric parallel 45^0 degrees lines bound the data points where the magnitude of phase difference, $\Delta\Phi=(\Phi_{uAB}-\Phi_P)$, is less than 35^0. A least square linear fit to the bounded data, shown as a thick line, has a slope of 45^0, but it crosses the $\Phi_{UAB} = 0$ line at $\Phi_P=-7.2^0$. This non-zero intercept indicates a constant phase lag of the pressure signal with respect to that of the PIV data, which is caused by differences in the location of the two sensors. We consider this phase lag to be real, considering that it represents about 2% of the full cycle, and that the physical separation between sensors is about 4 m, i.e. is about 4% of the 90m wavelength of 8s waves. This information can actually be used to estimate the direction of waves with respect to the PIV measuring plane. For run 103, this is about 60^0. Thus, when we compare the results of conditional sampling, we have to shift the phase of the pressure signal by the angle of the intercept. The magnitudes of phase shift for the three selected data sets are provided in Table 1. The shift remains unchanged for the first two series, since the orientation of

the platform is almost the same, but decreases to zero for run 105, as a result of re-orienting the light sheet with the changing flow direction.

When the values of $\Delta\Phi$, recalculated after shifting Φ_P, are within acceptable limits, it seems that our estimates of phase become reasonable. The total number of points bounded within two threshold levels, $\pm35^0$ and $\pm15^0$ (after shifting), out of a total of 3600 points, are also presented in Table 1. The numbers vary with turbulence intensity, characterized here by the Taylor microscale Reynolds number, Re_λ. For details how Re_λ is calculated, see Nimmo-Smith et al. (2005), and Luznik at al. (2005), the latter specifically for this series. For the more stringent threshold of $\pm15^0$, the number of points decreases to half of the data for two runs, and to almost one third for run 105. We are uncomfortable with removing such a large fraction of the data, and have opted to use $\Delta\Phi=\pm35^0$ as a criterion for compatibility.

Table 1: Statistics on the number of points satisfying two thresholds levels for $\Delta\Phi$, and the mean phase shift between velocity and pressure based phases.

Run #	Mean elevation (m)	Mean phase shift	# of data points $\Delta\Phi=\pm35^0$	# data points $\Delta\Phi=\pm15^0$	Re_λ
101	0.4	-7.5^0	3043	1856	242
103	1.5	-7.2^0	2987	1896	205
105	0.4	0	2431	1358	462

Several 400 s (out of 1200 s) time series associated with run 103 are presented in Figure 6. Figure 6a compares $\tilde{u}_{AB}$ to the pressure signal (P, expressed in meters of water) after shifting the latter by 7.2^0. The pressure records are also multiplied by 50 to present the data on the same scale. Figure 6b shows the corresponding corrected values of $\Delta\Phi$, along with the threshold levels used for sub-sampling the data, and Figure 6c shows the time history of $\langle u'u' \rangle$ and $-\langle u'w' \rangle$, as estimated from the structure function. The values of $\langle u'u' \rangle$ are shifted by 10 cm^2/s^2 for clarity. By comparing the plots one can see that in some of the instants where the phase exceeds the threshold level, the wave-induced pressure and velocity diminish. These low amplitude periods correspond to the familiar nodes (beating) created by superposition of two or more waves with slightly different frequencies. Yet there are other times where the phase difference and amplitude of wave induced motion are both large. A few of them occur during periods of high turbulence levels, such as the events marked by **x** and **xx** in Figure 6c, but others do not. More work is still needed to determine specific causes for some of the cases of phase mismatch. Nonetheless, for runs 101 and 103, 84% of the points fall within the threshold level, but only 67% satisfy the criterion for run 105, presumably due to the substantially higher turbulence levels.

The present analysis demonstrates how phase matching between time series of different sensors can be used as criteria for determining whether the phase calculations are reliable. Furthermore, it allows us to sub-sample the data using only points that satisfy the selected threshold level. However, since some of the cases that do not satisfy this condition are characterized by high turbulence levels, this criterion may create a bias. Thus, any sub-sampling should be performed with care. To show the effect of sub-sampling, Table 2 compares the stresses calculated using the entire time series to that of the sub-sampled data. As is evident, there are very little differences between values. Clearly, sub-sampling does not alter the Reynolds stress statistics.

Table 2: A comparison between Reynolds stresses calculated using the entire data and stresses calculated using the sub-sampled data.

	$\langle u'u' \rangle$		$\langle w'w' \rangle$		$\langle u'w' \rangle$	
run	all data	$\lvert\Delta\Phi\rvert < 35^0$	all data	$\lvert\Delta\Phi\rvert < 35^0$	all data	$\lvert\Delta\Phi\rvert < 35^0$
101	1.50	1.42	1.20	1.18	0.39	0.36
103	1.4	1.4	1.48	1.4	0.19	0.16
105	5.1	4.9	3.9	3.8	1.3	1.3

Conditionally Sampled Reynolds Stresses

Before concluding, this section examines the effect of wave phase on the turbulence statistics based on the sub-sampled data that satisfy the $\pm35^0$ threshold level. Figure 7 shows the variations of Reynolds stresses with phase for the three runs. For each case, we present the data conditionally sampled based on both Φ_{UAB} and Φ_P. The data are divided into ten 36^0 bins, but we also use a bi-directional running average of neighboring points to increase the sample size, and consistent with the threshold level. Several trends are evident from the results. First, both bases for conditional sampling show similar trends. Second, all the Reynolds stress components vary with wave phase, but most of the trends differ, consistent with the conclusions in Osborn et al. (2005). Repeated phenomena include: (1) a minimum in $\langle u'u' \rangle$ at or near $\Phi = 0$, the phase of maximum wave-induced horizontal velocity; and (2) variations close to 100% in the shear stress, and smaller variations, of less than 20%, in the normal stresses. The extent of differences in trends is puzzling. For example, Run 101 and 105 represent data recorded at the same elevation near the bottom (see Table 1), yet the trends with phase are substantially different. It is possible that the dissimilarity is caused by differences in orientation between mean flow and waves, or between the mean flow and bottom ripples. We do not know the answers to these questions, but they motivate more careful characterization of the local environment in future studies.

ACKNOWLEDGEMENTS

This project has been funded in part by NSF under grant No. OCE9819012 and in part by ONR, under grant No. N00014-95-1-0215. We are grateful to: Y. Ronzhes and S. King for their technical expertise in development of the equipment, the captain and crew of the R/V Cape Hatteras, A. Fricova and T. Kramer, for their assistance during deployments.

REFERENCES

Hristov, T., Friehe, C., and Miller, S., 1998, "Wave-coherent fields in air flow over ocean waves: identification of cooperative behavior buried in turbulence", *Physical Review letters*, Vol. 81(23), pp. 5245-5248.

Huang, N.E., Shen, Z, Long, S.R., Wu, M.C., Shih, H.H., Zheng, Q., Yen, N., Tung, C.C., and Liu, H.H., 1998, "The empirical mode decomposition and the Hilbert spectrum for

nonlinear and non-stationary time series analysis", *Proceedings of Royal Society of London, Series A*, Vol. 454, pp. 903-995.

Luznik, L., Gurka, R., Zhu, W., Nimmo Smith, W.A.M, Katz, J., Osborn, T.R., 2005, "Distribution of Energy Spectra, Reynolds Stresses, Turbulence Production and Dissipation in a Tidally Driven Bottom Boundary Layer", submitted to *Journal of Physical Oceanography*.

Nimmo Smith, W. A. M., Atsavapranee, P., Katz, J., and Osborn, T.R., 2002, "PIV Measurements in the bottom boundary layer of the coastal ocean", *Experiments in Fluids*, Vol. 33, pp. 962-971.

Nimmo Smith, W.A.M., Katz, J., and Osborn, T.R., 2005, "On the Structure of Turbulence in the Bottom Boundary Layer of the Coastal Ocean", in press, *Journal of Physical Oceanography*.

Osborn, T.R., Nimmo Smith, W.A.M., Luznik, L., and Katz, J., 2005, "Turbulence and waves in the bottom boundary layer of the coastal ocean", submitted to *Journal of Physical Oceanography*.

Roth, G.I., and Katz, J., 2001, "Five techniques for increasing the speed and accuracy of PIV interrogation", *Measurements Science and Technology*, Vol. 16, pp. 1568-1579.

Thais, L., and Magnaudet, J., 1996, "Turbulent structure beneath surface gravity waves sheared by the wind", *Journal of Fluid Mechanics*, Vol. 328, pp. 313-344.

Trowbridge, J.H., 1998, "On a Technique for Measurement of Turbulent Shear Stress in the Presence of Surface Waves", *Journal of Atmospheric Oceanic Technology*, Vol. 15, pp. 290-298.

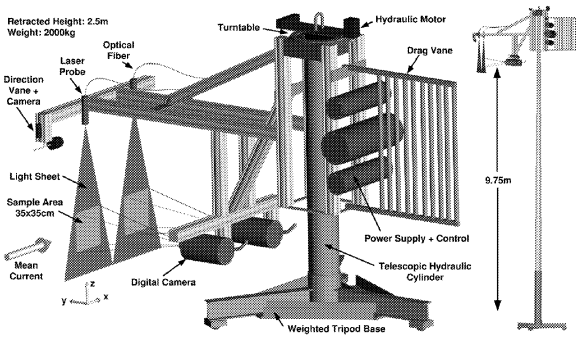

Figure 1: Drawing of the submerged components of the PIV system.

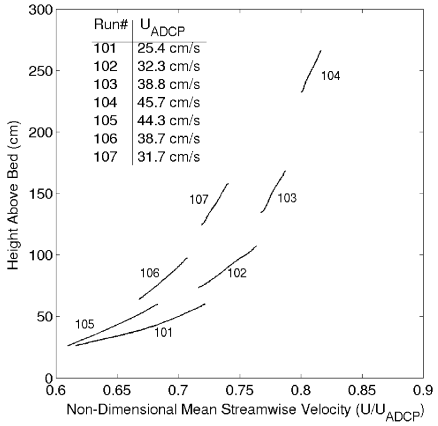

Figure 2: Mean streamwise velocity profiles.

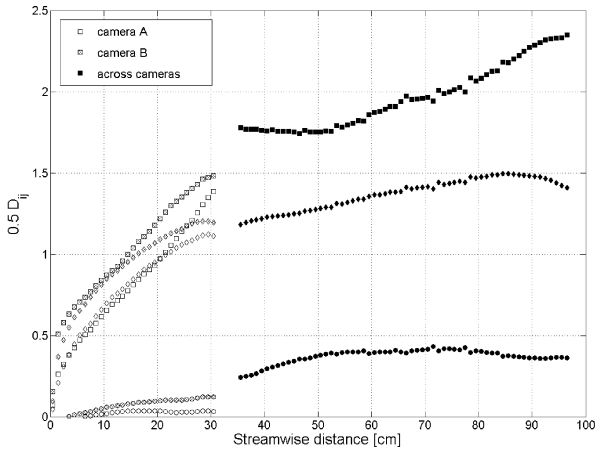

Figure 3: Sample of the 2nd order structure function, (run 101). -<u'w'> ○, <w'w'> ◊, <u'u'> □.

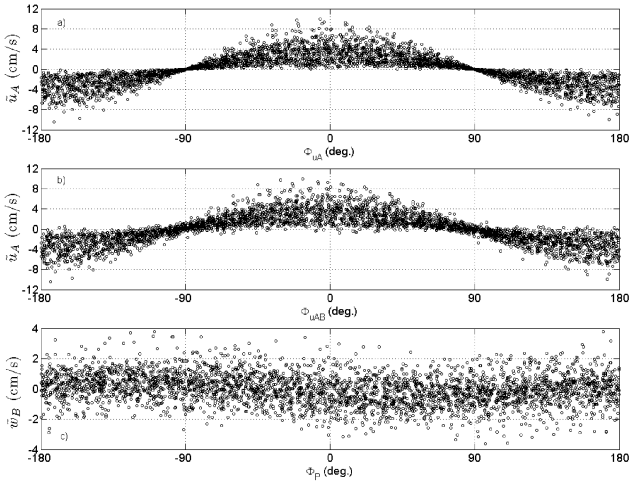

Figure 4: Sample scatter plots (run 103) of the velocity components as a function of the instantaneous phase.

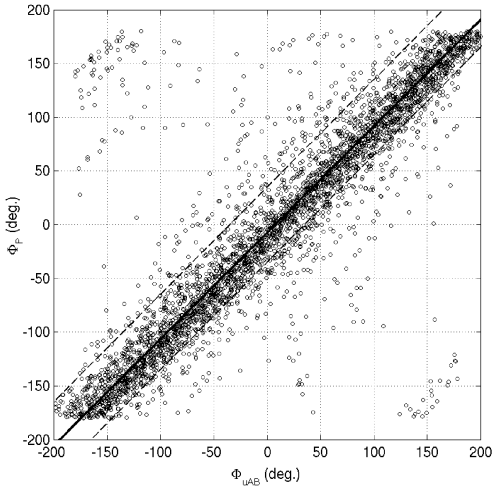

Figure 5: Scatter plot of the instantaneous phase from two different data sources (run 103): pressure record Φ_P, and Φ_{uAB} based on average horizontal velocity from two cameras.

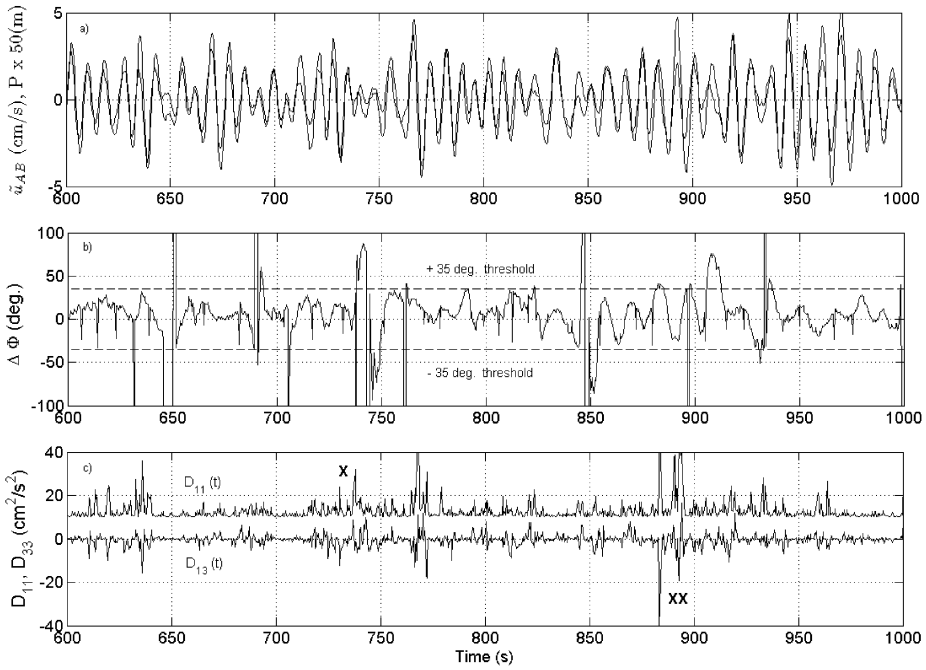

Figure 6: Sample partial time history (run 103). a) Time series of pressure and $\tilde{u}_{AB}$. The pressure signal is phase shifted by 7.2 degrees. b) Phase difference $\Delta\Phi=(\Phi_{uAB}-\Phi_P)$, c) Time series of $D_{11}(t)$ and $D_{13}(t)$.

a) b)

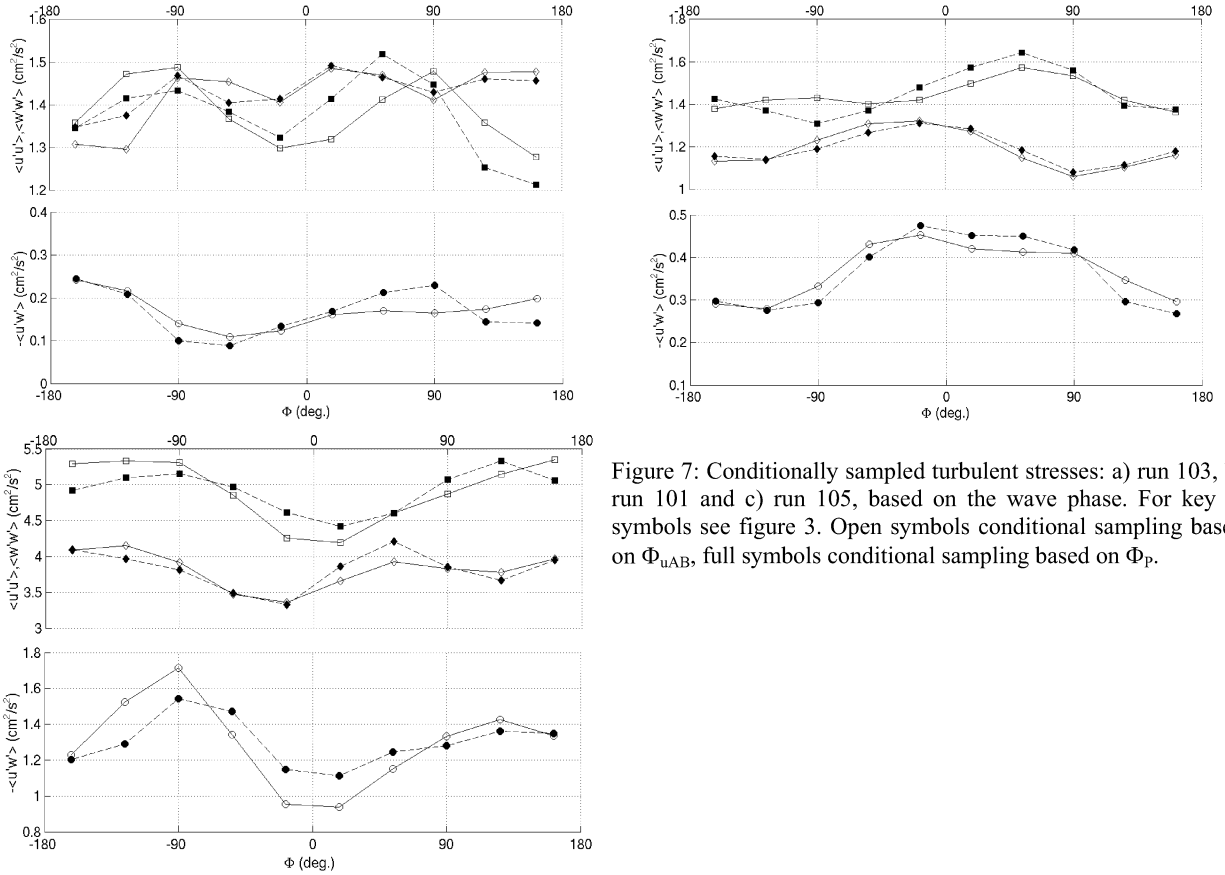

Figure 7: Conditionally sampled turbulent stresses: a) run 103, b) run 101 and c) run 105, based on the wave phase. For key to symbols see figure 3. Open symbols conditional sampling based on Φ_{uAB}, full symbols conditional sampling based on Φ_P.